Chapter 2
Source/Drain Junctions in Germanium: Experimental Investigation

In this chapter, the fabrication of shallow junctions in germanium is investigated experimentally, targeting application in a scaled germanium MOSFET technology.

2.1 Introduction

Improvements in the microelectronic industry over the past decades have relied heavily on a continuous effort to overcome the difficulties of device shrinking [75]. Germanium is considered as an attractive high mobility substrate for high performance CMOS applications. One critical issue towards the establishment of a scaled Ge-based technology is the ability to fabricate shallow, low-resistive junctions in this material. Consequently, a systematic investigation of the diffusion and activation behavior of ion-implanted (I/I) dopants in Ge substrates during drive-in anneal is required.

Regarding p-type junctions, existing studies have focussed mainly on boron, also the dominant p-type dopant in Si technology. An interesting alternative for p-type doping of germanium is gallium: its higher atomic mass reduces both the straggle and ion-channeling during I/I, leading to a more abrupt as-implanted profile (compared to the lighter B). For this reason, the implantation of Ga and its behavior during subsequent annealing will be investigated in this chapter. In a second study, ion-implanted boron in Ge will be studied in sub-30 nm junctions.

Regarding n-type junctions, phosphorus and arsenic both suffer from significant concentration-enhanced diffusion in germanium through the formation of arsenic- or phosphorus-Vacancy complexes, at concentrations in excess of $2–5 \times 10^{19}$ cm^{-3}. As such, the fabrication of ultra-shallow n-type junctions in Ge requires limiting the activation anneal's thermal budget while at the same time, a high temperature is required to achieve a high electrically active concentration. Attempting to combine these two competing requirements, the feasibility of millisecond laser annealing (LSA) to fabricate ultra-shallow low-resistive n-type junctions is investigated, using As.

G. Hellings, K. De Meyer, *High Mobility and Quantum Well Transistors*,
Springer Series in Advanced Microelectronics 42, DOI 10.1007/978-94-007-6340-1_2,

Finally, this chapter intends to explore opportunities for junctions in high mobility materials by benchmarking against existing literature data and against the ITRS requirements for the upcoming technology nodes.

2.2 p-Type Junctions

2.2.1 Furnace Annealed Gallium Junctions

The goal of this section is to investigate the behavior of ion-implanted gallium and its subsequent annealing at different temperatures in preamorphized (α-Ge) and crystalline germanium (c-Ge). To this end, the as-implanted profiles, electrical activation, diffusion and recrystallization process will be discussed.

2.2.1.1 Experimental Details

Czochralski-grown 100 mm diameter, 350 µm-thick, (100)-oriented, n-type bulk Ge wafers were obtained from Umicore. On one set of wafers, a Preamorphization Implant (PAI) was performed using Ge at an energy of 200 keV and with a dose of 10^{15} cm^{-2}. This PAI results in a 190 nm-thick amorphized layer on these wafers. Subsequently, Ga was implanted at different energies (40 and 80 keV) with a dose of 3×10^{15} cm^{-2} with a 7° tilt with respect to the wafer normal. On another set of wafers, Ga was directly implanted without a preceding PAI-step. Immediately after the I/I, all wafers were capped with a protecting 20 nm SiO_2 layer. The annealing was performed in N_2 atmosphere in a *Heatpulse 610* rapid thermal annealing (RTA) system at temperatures between 300 and 700 °C for 60 s. The chemical dopant concentrations were studied by Secondary-Ion Mass Spectroscopy (SIMS). The electrical activation of Ga was analyzed by sheet resistance measurements with a conventional four-point probe (4PP) system, the variable probe spacing technique (VPS, [25]) and a micro-four-point probe system (μ4PP, [112]). The implant-induced damage and residual disorder after annealing were studied with transmission electron microscopy (TEM).

2.2.1.2 Physical Characterization

Figure 2.1 shows the as-implanted Ga profiles with energies of 40 and 80 keV and a dose of 3×10^{15} cm^{-2} in both α-Ge and c-Ge. In the c-Ge, a channeling tail is clearly distinguishable at concentrations below 10^{18} cm^{-3}. The as-implanted profiles (in α-Ge) were fitted with Pearson distribution curves [5] of which the resulting moments are also given.

The implantation of 40 keV Ga with a dose of 3×10^{15} cm^{-2} amorphized the c-Ge to a depth of 58 nm, as shown by the TEM micrograph in Fig. 2.2(a).

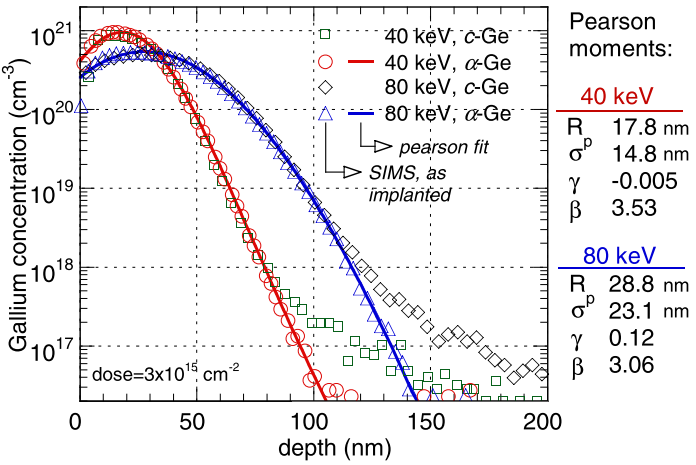

Fig. 2.1 Chemical concentration profiles as a function of depth for Ga, as implanted in the α-Ge and c-Ge samples (40 and 80 keV 3×10^{15} cm^{-2}). The profiles in α-Ge were also fitted with Pearson distribution curves

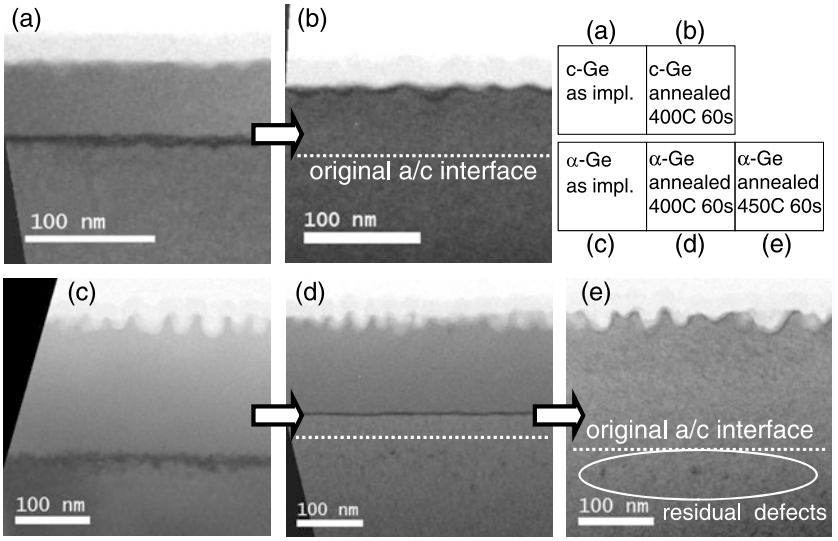

Fig. 2.2 Cross-sectional TEM of 40 keV 3×10^{15} cm^{-2} Ga implanted in c-Ge (*top*) and α-Ge (*bottom*)

The 80 keV implant is expected to yield an amorphous layer of 92 nm, based on Monte Carlo simulations—see Chap. 3). Full recrystallization occurs after the 60 s anneal at 400 °C (Fig. 2.2(b)). The Ge surface appears to be quite rough, even before the recrystallization. This can be attributed to vacancy migration [76] because the I/I was performed prior to depositing the protecting SiO_2 cap layer. While this

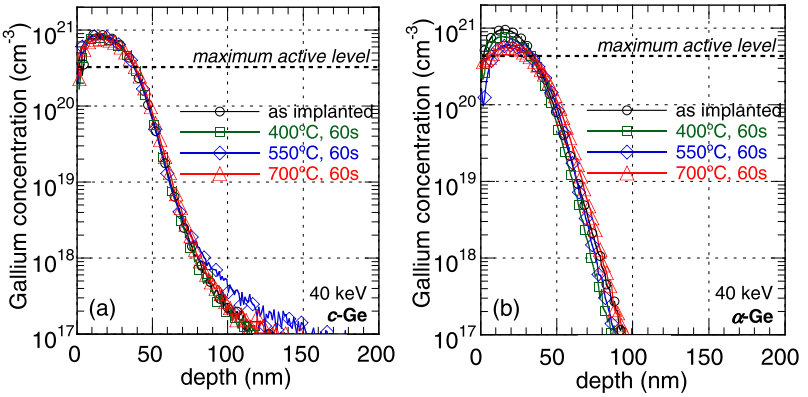

Fig. 2.3 Chemical concentration profiles as a function of depth for Ga (40 keV 3×10^{15} cm^{-2}), as-implanted and annealed at 400, 550 and 700 °C for 60 s in *c*-Ge and α-Ge

surface roughening for high-dose, heavy-ion I/I at room temperature is undesirable for device fabrication, it can be avoided by cooling the substrate during the I/I-step (hence suppressing the vacancy diffusion). In the α-Ge samples, the roughening is even more severe due to the 200 keV Ge PAI, as shown in Fig. 2.2(c). Here, only 40 nm of Ge was regrown during the 400 °C anneal (Fig. 2.2(d)), indicating a slower regrowth than in the *c*-Ge sample and as reported by Csepregi et al. in [29]. Full recrystallization however was achieved with the 450 °C anneal, while residual crystal damage can still be observed below the original a/c interface, agreeing with the observations by Hickey et al. in [65] (Fig. 2.2(e)).

To investigate the diffusion behavior, the Ga profile was analyzed in SiO_2-capped samples annealed at 400, 550 and 700 °C for 60 s using SIMS. The corresponding profiles are presented in Fig. 2.3(a) and (b) for *c*-Ge and α-Ge substrates respectively. As shown in Fig. 2.3(a), no diffusion could be observed in the *c*-Ge sample for temperatures up to 700 °C, confirming the reduced diffusivity of group III elements in Ge reported in [120]. Within the accuracy of the SIMS analysis, the total implanted dose was fully retained in the sample during the anneal. Also in the α-Ge samples, no diffusion was observed up to 700 °C. However, the peak Ga concentration dropped steadily from 9×10^{20} to 5.5×10^{20} cm^{-3} with increasing temperature. In the 550 °C sample, only 70 % of the total implanted dose was retained (no additional dose loss was observed by further increasing the RTA temperature up to 700 °C).

To find an explanation for this, the recrystallization was analyzed in more detail. The thicker amorphous layer (190 nm) and the observed slower crystal regrowth imply that Ga remains longer in the amorphous phase for the α-Ge samples. This also implies that Ga is still in the amorphous phase at higher temperatures during the ramp-up (rate 20 °C/s) of the high-temperature RTA anneals. Illustrating this, the recrystallization process was calculated in more detail, using the temperature-dependent regrowth model from [29] (accounting for the slower regrowth observed

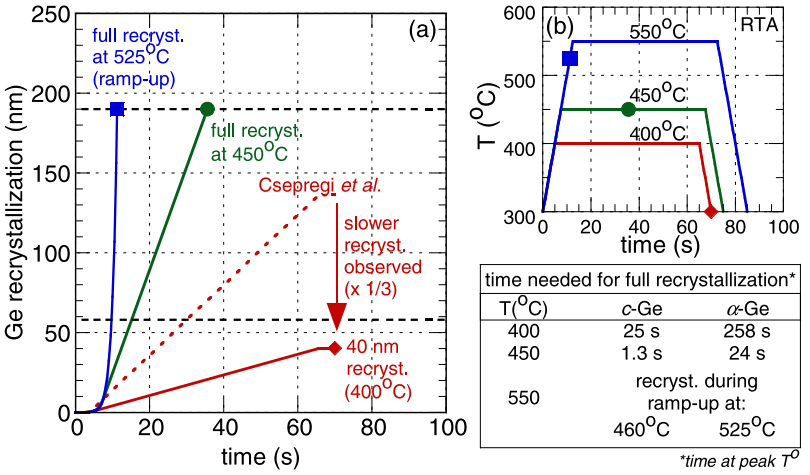

Fig. 2.4 (**a**) Calculated recrystallization thickness as a function of time for the α-Ge samples for (**b**) three different anneal temperatures. The regrowth model from Csepregi et al. [29] was modified to account for the slower regrowth observed in our α-Ge samples (see text). Full recrystallization is expected to occur after 24 s (450 °C anneal) or during the ramp-up phase of the 550 °C anneal. The symbols link the end of each regrowth curve in (**a**) to a time-T° point in (**b**). Finally, *a table* shows the estimated annealing time required for full recrystallization

during the TEM analysis in the α-Ge samples). The results of these calculations are shown in Fig. 2.4:

- The 400 °C RTA anneal resulted in a 40 nm recrystallization based on the TEM analysis of the α-Ge samples. At this rate, an annealing time of 258 s would be required for full recrystallization of the 190 nm thick amorphous Ge layer. For the *c*-Ge sample, the 400 °C RTA anneal resulted in full recrystallization of the 58 nm (see Fig. 2.2(b)). Assuming the regrowth velocity from [29], one can estimate that the amorphous layer is fully recrystallized after only 25 s at 400 °C.
- The 450 °C RTA anneal resulted in a full recrystallization after 24 s for the α-Ge sample, in contrast to only 1.3 s for the *c*-Ge sample, where the amorphous layer almost fully recrystallizes during the ramp-up towards 450 °C.
- The 550 °C RTA anneal achieves full recrystallization of the amorphous layer during the ramp-up phase. This occurs at a temperature of 525 °C for the α-Ge sample and at 460 °C for the *c*-Ge sample.

Note that these estimates assume a 3× slower regrowth velocity for the α-Ge samples, as observed in our samples. Without this assumption, the difference between the *c*-Ge and α-Ge recrystallization times would be smaller (although still substantial).

With these considerations in mind, enhanced Ga diffusion in the amorphous Ge phase explains our observations: during the 400 °C anneal, Ga is present in the amorphous Ge phase at the same temperature (i.e. 400 °C) in the α-Ge and *c*-Ge samples. This corresponds with the small dose loss observed for the α-Ge sample

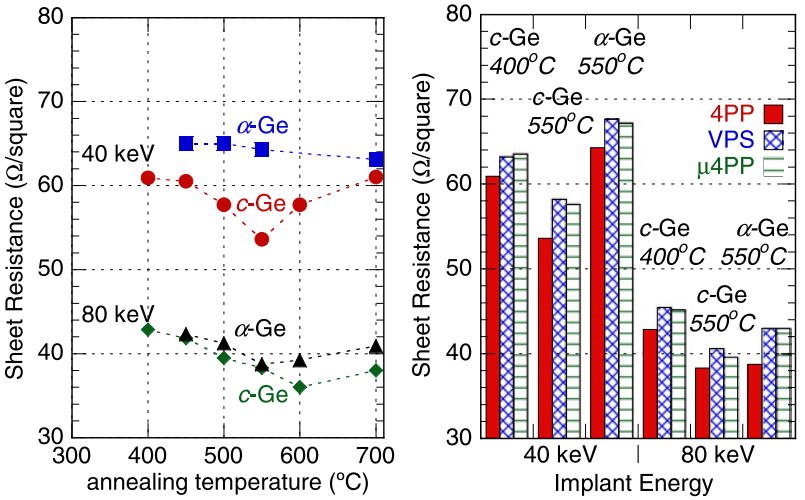

Fig. 2.5 (**a**) Sheet resistance of Ga junctions formed by I/I (40 and 80 keV) in α-Ge and c-Ge, as a function of annealing temperature measured with the conventional 4PP. (**b**) Sheet resistance for selected samples measured with the conventional 4PP, the VPS technique and the μ4PP system

(Fig. 2.3(b)), which can be attributed to the longer time spent at this temperature. During the higher temperature anneals, Ga remains in the amorphous Ge phase until the wafer reaches a temperature of 525 °C in α-Ge substrates, in contrast to only 460 °C for c-Ge. The fact that no additional dose loss is observed for a 700 °C anneal, in comparison to the 550 °C one, also indicates that the observed dose loss is linked to the identical feature of these two anneals, i.e. the ramp-up phase of the RTA-anneal. However, to fully confirm this model, additional dedicated experiments would be needed to rule out any effect related to the surface morphology (e.g. roughness).

2.2.1.3 Electrical Characterization

The electrical activation of Ga-doped Ge was studied by sheet resistance measurements (R_{sh}) using three techniques (4PP, VPS and μ4PP). While the relative simplicity of the conventional 4PP tool is an advantage, the probe penetration in Ge can be quite high (up to about 200 nm, depending on probe pressure [26]). Since the Ga junctions under investigation are considerably shallower than 200 nm, the concern is that the probe-needles would pierce the junction, yielding erroneous results. This was indeed found to be the case since no reliable, reproducible R_{sh} could be obtained using the conventional 4PP technique on our samples. Attempting to circumvent this, a second set of 4PP measurements was carried out while leaving the protecting SiO_2 cap layer on the sample. Apparently, this extra layer reduced the 4PP probe penetration enough to allow reproducible R_{sh} measurements: Fig. 2.5(a) shows the annealing temperature dependence of R_{sh}, for the Ga junctions fabricated

in α-Ge and c-Ge. The sheet resistance remains rather constant for both implant energies as soon as the samples are fully recrystallized: the R_{sh} variation over the entire temperature range is only 10 %, with an optimum around 550 °C. This implies that a high Ga activation is already obtained at rather low temperatures (400 °C). Finally, the lowest R_{sh} value is obtained at a temperature of 500–600 °C.

In order to confirm the validity of our R_{sh} measurements with the 4PP-tool (leaving the SiO_2 layer present), VPS and μ4PP measurements were as well performed on selected samples (without the SiO_2 cap). The R_{sh} values are found to be consistent across these three techniques and results are plotted in Fig. 2.5(b): the difference between the VPS and μ4PP values is generally smaller than a few percent, while the 4PP measurements yield the same trend but give slightly lower values (5 %).

From the SIMS analysis of the annealed samples, the VPS-based R_{sh}, and a concentration-dependent mobility model for Ga-doped germanium [50], an active concentration level can be calculated. This calculation yields a maximum active concentration level of 4.4×10^{20} and 3.3×10^{20} cm^{-3} for Ga implanted into c-Ge and α-Ge respectively (the methodology of this calculation is explained in [123]). The accuracy of these levels is mainly determined by the uncertainty on the mobility model used, which dates back to 1962. A more recent mobility model is available for B-doped Ge [98], yielding slightly lower maximum active concentration levels (2.6×10^{20} cm^{-3}). However, Hall-mobility measurements carried out on our own samples tend to agree with the original model [63]. Finally, the observed active Ga concentration level is very similar to the solid solubility limit of Ga in Ge (4×10^{20} cm^{-3}, [148]). A similar correlation with the solid solubility limit was previously observed for the active concentration level of B in Ge [123, 152].

2.2.2 Furnace Annealed Boron Junctions

The goal of this section is twofold. Firstly, ion-implanted boron junctions in Ge and their behavior during subsequent furnace anneals are investigated. Secondly, the boron junctions are co-implanted with arsenic and fluor, thus creating samples resembling the integration of B junctions in a bulk Ge MOSFET flow.

2.2.2.1 Experimental Details

Boron junctions were fabricated using n-type, 200 mm diameter, (100)-oriented Si wafers on which a relaxed epitaxial Ge layer was grown (1.5 μm thick, threading dislocation density approx. 2×10^7 cm^{-2}). All wafers (D02, D05 and D11 are discussed in this section) received phosphorus well implants, yielding an n-well with a doping concentration of 3×10^{17} cm^{-3}. Two wafers (D02 and D05) were implanted with As (80 keV, 5×10^{13} cm^{-2}, 15° tilt), followed by a F implant on D05 (4.3 keV, 1.6×10^{15} cm^{-2}, 7° tilt). After these I/I steps, the wafers were capped with a 10 nm thick protective SiO_2 layer. Subsequent annealing was performed in

Table 2.1 Overview of relevant quantities for the samples used in this study

Wafer number	D11	D02	D05
n-well (multiple P implants & anneal)	×	×	×
I/I: As 80 keV, 5×10^{13} cm^{-2} 15° tilt		×	×
I/I: F 4.3 keV, 1.6×10^{15} cm^{-2} 7° tilt			×
I/I: B 2.4 keV, 8×10^{14} cm^{-2} 7° tilt	×	×	×
SiO_2 deposition (10 nm)	×	×	×
RTA anneal 550 °C, 5 min, N_2	×	×	×
R_{sh} (4PP-tool)	–	failed	–
R_{sh} (VPS-technique)	–	83.5[a]	–
R_{sh} (μ4PP)	488.2	153.2	425.6

[a] R_{sh} value is too low due to probe penetration (measuring the substrate in parallel with the B-doped layer)

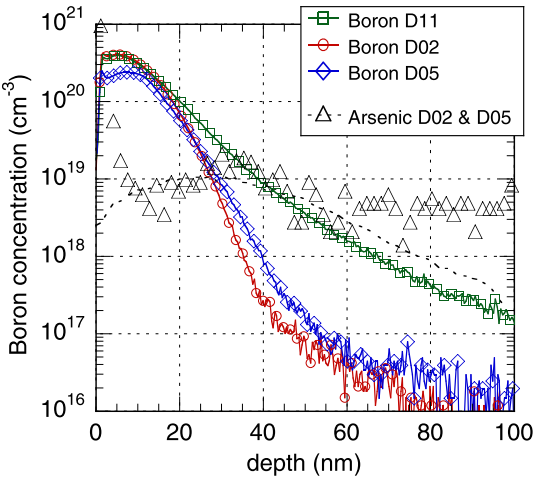

Fig. 2.6 Chemical concentration profiles as a function of depth for the boron (2.4 keV 8×10^{14} cm^{-2}), implanted in Ge and annealed at 550 °C for 5 min. Processing details can be found in Sect. 2.1

N_2 atmosphere in a *Heatpulse 610* rapid thermal annealing (RTA) system at 550 °C for 5 min. The chemical dopant concentration was studied by secondary-ion mass spectroscopy (SIMS), the electrical activation of B was analyzed by sheet resistance measurements with a conventional four-point probe (4PP) system, the variable probe spacing technique (VPS, [25]) and a micro-four-point probe system (μ4PP, [112]). The processing details of these samples are summarized in Table 2.1.

2.2.2.2 Physical Characterization

The chemical dopant concentration profiles in these wafers were analyzed using SIMS (Fig. 2.6). In wafer D11, which only received the B I/I, a pronounced tail is

visible. This can be attributed to ion channeling during the implant and results in a rather deep junction. In wafer D02, the B profile is much shallower as a result of the preceding As implant. The implantation of As with a dose of 5×10^{13} cm^{-2} amorphizes the Ge to a depth of 37 nm (as measured using spectroscopic ellipsometry), thus eliminating ion-channeling during the subsequent B implant. As a result, the junction depth is reduced to 27 nm. Finally, in wafer D05, where F was implanted as well, considerable B dose-loss and slight in-diffusion can be observed. This reduces the total retained B dose and increases the junction depth again compared to sample D02 to $X_J = 30$ nm.

2.2.2.3 Electrical Characterization

On these B junctions, the sheet resistance R_{sh} was measured by conventional 4PP, the VPS technique and the μ4PP system. The first two techniques, while successful for the deeper Ga junctions in Sect. 2.2.1, did not deliver reliable results on the B samples (with and without the oxide cap on the sample). This is caused by the fact that these B junctions are even shallower and 4PP needles penetrate through the junction (contacting also the substrate). Consequently, the junction sheet resistance is measured in parallel with the substrate yielding a too low R_{sh}-value. Reliable measurements however could be obtained using the penetration-less μ4PP tool (oxide cap removed—see Table 2.1).

For wafer D11, R_{sh} is found to be 488.2 Ω/sq., corresponding to a calculated maximum active B concentration level of 1×10^{19} cm^{-3} (using the same methodology and mobility model as in Sect. 2.2.1.3). Similar low active concentration levels have been reported before for B implants into c-Ge and subsequent RTA annealing [123]. In order to reach a higher active boron concentration, Solid Phase Epitaxial Regrowth (SPER) is required: the full recrystallization of amorphous Ge has been reported to yield active B concentrations up to 6×10^{20} cm^{-3} [98], depending on anneal conditions. In wafer D02, the amorphous layer created by the As implant fully recrystallizes during the anneal. As such, a high active boron concentration level (4×10^{20} cm^{-3}) is obtained through SPER resulting in a low $R_{sh} = 153.2$ Ω/sq. Finally, in wafer D05, a higher R_{sh} is measured (425.6 Ω/sq.). This can be explained by the significant out-diffusion of B during the RTA anneal. As a result, the calculated maximum active concentration level drops to 1.8×10^{20} cm^{-3}.

2.2.3 Conclusions

In the previous section, gallium and boron were studied as possible p-type dopants in Ge. For Ga, a high active concentration (4.4×10^{20} cm^{-3}) was obtained without preceding Ge preamorphization (PAI) of the substrate. The low activation temperature (400 °C), combined with the absence of Ga-diffusion up to a temperature

of 700 °C, make Ga junctions in crystalline Ge promising candidates for implementation in a High Performance, Short-Channel Ge technology. In the amorphous Ge phase, an increased Ga diffusivity and lower active concentration was observed following RTA-anneals above 400 °C. B junctions were fabricated showing similar high active concentrations (4×10^{20} cm^{-3}) for a junction depth as small as 27 nm. This however required a preamorphization of the Ge lattice prior to the B I/I such that B is efficiently incorporated through the mechanism of solid phase epitaxial regrowth into the Ge lattice during the RTA anneal. Finally, co-implanting with fluor caused significant B dose loss during the RTA anneal, yielding a 2× lower active concentration.

2.3 n-Type Junctions

2.3.1 Laser Annealed Arsenic Junctions

In contrast to their p-type counterparts [70, 98], RTA-annealed n-type junctions in Ge suffer from significant concentration-enhanced diffusion (using phosphorus or arsenic as dopant, [14, 36]). As such, the fabrication of ultrashallow n-type junctions requires limiting the activation anneal's thermal budget. At the same time, a higher temperature is required to achieve a high electrically active concentration. These two competing requirements have led to the use of ultrafast heat-treatment methods such as flash-assisted annealing (FLA, [51, 117, 132]) and millisecond laser annealing (LSA, [68, 150]). In this section, the feasibility of LSA to fabricate ultrashallow, low-resistive As junctions in Ge is studied. More specifically, the effects of the laser peak wafer temperature and the combination with a preamorphization implant (PAI) will be discussed.

2.3.1.1 Experimental Details

Arsenic junctions were fabricated using p-type, 300 mm diameter, (100)-oriented Si wafers on which a relaxed epitaxial Ge layer was grown (1.5 μm thick, threading dislocation density approx. 2×10^7 cm^{-2}). After growing a protective 2 nm GeO_2 layer, they received a boron n-well doping up to 3×10^{17} cm^{-3}, followed by a Ge PAI (20 keV, 2×10^{14} cm^{-2}) on selected samples, yielding an amorphized layer of 25 nm. Arsenic was implanted at an energy of 5 keV up to a dose of 5×10^{14} cm^{-2}. The samples then received millisecond laser annealing. The laser spot measured 1.1 cm × 75 μm and scans the wafer left-to-right at a speed of 75 mm/s (two consecutive scans). During the laser illumination, a wafer preheating is applied (250 °C) to reduce thermal stress arising from the localized laser heating. No absorber layer was deposited to assist in the laser anneal. Multiple regions (each measuring at least 5 × 5 cm) were illuminated, whereby the laser energy was varied in steps of 100 °C to reach peak wafer temperatures up to 900 °C (close to Ge's melting temperature

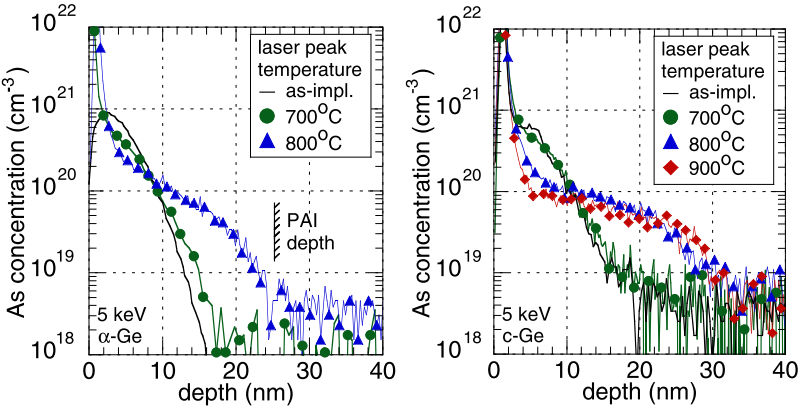

Fig. 2.7 Chemical concentration profiles as a function of depth for the As junctions (5 keV 5×10^{14} cm^{-2}), as-implanted in preamorphized (**a**) and crystalline (**b**) Ge and after LSA anneal

$T_{melt} = 937\,°C$). This temperature staircase was calibrated by observing the onset of melting on the *c*-Ge wafers and assuming a linear dependency. Following this assumption, reported peak wafer temperatures should be considered an estimate. The chemical dopant concentrations was studied by secondary-ion mass spectroscopy (SIMS), the electrical activation of As was analyzed by sheet resistance measurements using the micro-four-point probe system (μ4PP, [112]). Additionally, Hall mobility measurements were also performed using the same system. An overview of the different samples and measured quantities is given in Table 2.2. The implant-induced damage and subsequent recrystallization were studied with transmission electron microscopy (TEM) and spectroscopic ellipsometry.

2.3.1.2 Physical Characterization

To investigate the diffusion behavior, the chemical As concentration was analyzed using SIMS. The resulting concentration profiles have a rather high background noise level (range mid-10^{18} cm^{-3}). This is due to mass interference of the ^{75}As with ^{74}Ge-^{1}H (^{74}Ge is the main Ge isotope). Figure 2.7(a) (α-Ge wafers) and Fig. 2.7(b) (*c*-Ge wafers) contain the resulting As concentration profiles for the laser annealed junctions for LSA wafer peak temperatures of 700, 800 and 900 °C. No significant As diffusion is observed up to a peak temperature of 700 °C, while considerable in-diffusion is present for samples annealed at 800 and 900 °C. The box-like profile after diffusion in the samples suggests that the concentration-enhanced diffusion mechanism (observed in RTA experiments, [125]) still applies. However, As diffusion seems to be rather independent of temperature in the range 800–900 °C, resulting in very similar As profiles for these annealing conditions. This enhanced diffusion leading to a box-like As profile is not observed on the α-Ge samples, where recrystallization occurs during LSA. A similar effect was seen in Si technology for

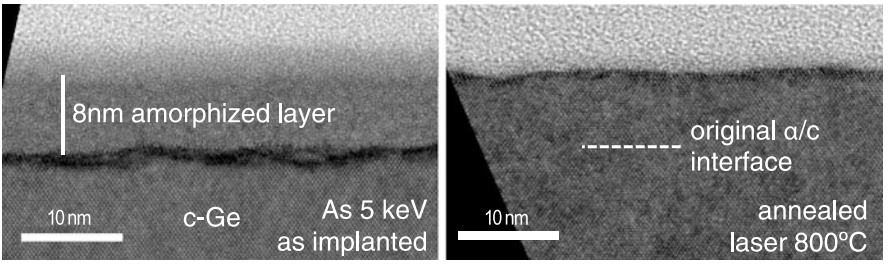

Fig. 2.8 Cross-sectional TEM of As-implanted *c*-Ge before (**a**) and after an 800 °C LSA anneal (**b**) showing full recrystallization

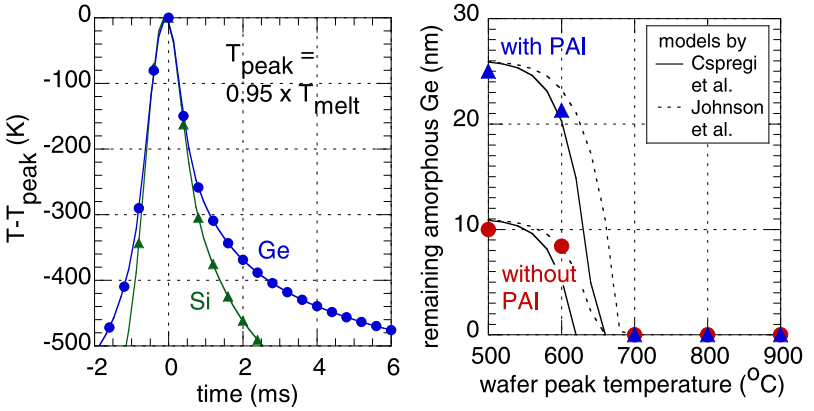

Fig. 2.9 (**a**) TCAD-simulated wafer surface temperature as a function of time for Si and Ge (peak temperature set to 95 % of T_{melt}). (**b**) Measured remaining thickness of the amorphous layer created by the ion implant after LSA anneal. The observed recrystallization is compared to literature using the TCAD-generated temperature profile

laser annealed As junctions, where PAI gives rise to a higher electrical activation [106]. Even though the same laser power was applied to the *c*-Ge and α-Ge samples (see Table 2.2), localized surface melting was observed on the 900 °C α-Ge sample, yielding a highly non-uniform junction, unsuited for further analysis. This observation may be caused by a decrease in surface reflectivity due to the amorphization, hence increasing the energy absorbed by the sample during LSA. Consequently, the estimated peak temperature for the α-Ge samples may be slightly higher than that of their *c*-Ge counterparts. Alternatively, this may be due to a difference in melting temperature between amorphized and crystalline Ge (as previously observed for Si in [143]).

The As implant results in amorphized Ge to a depth of 8 nm, as shown by the TEM micrographs in Fig. 2.8. Full recrystallization is observed after LSA at 800 °C. No residual crystal damage is observed at the original a/c interface. In contrast, recrystallization during LSA is known to be more cumbersome in Si, requiring addi-

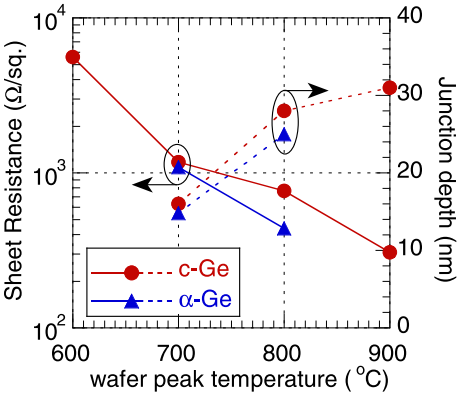

Fig. 2.10 Sheet resistance as measured with the μ4PP and junction depth for the laser annealed As junctions as a function of LSA peak temperature

tional treatments to cure remaining crystallographic defects [129]. To further investigate the recrystallization during LSA, a $T(t)$-profile was obtained using thermal TCAD simulations [128] to which the relevant material parameters for Ge were added (thermal conductivity [49], specific heat capacity [107]). For comparison, the same simulation was performed on Si substrates, using available default parameters. A typical $T(t)$-profile is plotted in Fig. 2.9(a). The LSA power was chosen to result in a peak wafer temperature $T_{peak} = 0.95 \times T_{melt}$. Note the striking similarity in the $T(t)$ profile in both materials, despite the difference in material parameters (the divergence from 2–6 ms is due to a different preheat temperature during LSA). This leads to the conclusion that the properties of the LSA tool (laser spot size, scanning speed, preheat temperature, etc.) are dominantly responsible for the shape of the temperature profile as a function of time.

The thickness of the remaining amorphous Ge as a function of T_{peak} was also measured with spectroscopic ellipsometry. Given the simulated $T(t)$ profiles, these can be compared to the expected recrystallization based on available Ge recrystallization models [29, 77] in Fig. 2.9(b). Firstly, reasonable agreement is obtained between the measurements and the regrowth models. Secondly, the amorphous layer is observed to be fully recrystallized after laser anneal with $T_{peak} = 700\,°C$, which is in line with the recrystallization models. Thirdly, whereas high P concentrations were shown to retard the regrowth substantially in [131], similar behavior could not be observed in the presence of As during our experiments. However, dedicated experiments would certainly be required to study this in-depth.

2.3.1.3 Electrical Characterization

The electrical activation of the arsenic junctions was studied through sheet resistance and Hall mobility measurements. Both of these were carried out using the μ4PP tool as described in [113], since the probe needles of a regular 4PP tool would definitely penetrate too deep into the Ge (given that 4PP already failed for deeper B junctions in Sect. 2.2.2) [26]. The measured and extracted quantities discussed in this section are listed in Table 2.2. The reported sheet resistances result

Table 2.2 Overview of relevant quantities for the samples used in this study

Sample number	Substrate type	Peak T (°C)	Laser energy (J/cm^{-2})	X_J (nm)	R_{sh} (Ω/sq.)
1	c-Ge	700	43.9	16	1173 ± 3 %
2	c-Ge	800	53.6	28	765 ± 2 %
3	c-Ge	900	63.4	31	308 ± 0.3 %
4	α-Ge	700	43.9	15	1089 ± 5 %
5	α-Ge	800	53.6	25	438 ± 3 %
6	α-Ge	900	63.4	*surface melting*	

Sample number	Hall μ (cm^2/Vs)	Hall electron density (cm^{-2})	Activation (%)	Calculated active concentration (cm^{-3})
1	80 ± 9 %	6.67×10^{13}	13	2.4×10^{19}[a]
2	96 ± 6 %	8.54×10^{13}	17	1.8×10^{19}
3	126 ± 5 %	1.61×10^{14}	32	5.0×10^{19}
4	76 ± 15 %	7.54×10^{13}	15	2.7×10^{19}[a]
5	111 ± 6 %	1.28×10^{14}	26	4.6×10^{19}
6	*no data—surface melting observed*			

[a]Uncertainties on the mobility model and especially on the SIMS close to the surface can cause large (± 50 %) errors on the calculated activation level for the shallowest junctions

from multiple measurements on random locations for each sample and vary within 5 %, indicating that a uniform junction was formed, as in previous work [114]. The sheet resistance (R_{sh}) and the junction depth (X_J) as a function of peak wafer temperatures are plotted in Fig. 2.10. Firstly, in all investigated samples, a higher peak temperature is found to result in a deeper junction with a lower R_{sh}. Secondly, the α-Ge samples show lower R_{sh} in combination with a reduced X_J, indicating a higher electrical activation level. Note that X_J is extracted from the SIMS profile at a concentration of 10^{19} cm^{-3} (this is necessary because of the mid-10^{18} cm^{-3} noise-level on the SIMS).

From the SIMS analysis, R_{sh} and a concentration-dependent mobility model of As-doped germanium [44], an active concentration level was calculated. For the c-Ge samples, a maximum active concentration level of 5.0×10^{19} cm^{-3} was found for the 900 °C laser anneal. Comparing the α-Ge and c-Ge samples at 800 °C, the effect of the Ge PAI and the subsequent SPER can be seen: the maximum active As level increases from 1.8×10^{19} to 4.6×10^{19} cm^{-3}. This higher electrically active As concentration level can be explained by considering that As deactivation and diffusion in Ge are both known to be caused by the formation of mobile arsenic-vacancy (As-V) complexes [22]. As such, the formation of As-V complexes results in As de-activation and diffusion in the c-Ge samples, while As-V complexes are formed in lower concentrations in α-Ge samples due to the SPER. Another indication for this model is that the 900 °C c-Ge sample shows very little additional As

diffusion with respect to the 800 °C c-Ge sample, consistent with theoretical calculations [22] predicting that As-V complexes are increasingly unstable at temperatures above 700–800 °C.

The electrically active As concentration of 5.0×10^{19} cm^{-3} in the 900 °C c-Ge sample is similar to the solid solubility limit of As in Ge at this temperature (i.e. 6×10^{19} cm^{-3} [134]), suggesting an efficient incorporation of As into the Ge lattice. The active As concentration also exceeds the level generally achieved using RTA annealing techniques [24].

The observed Hall mobility measurements (with the μ4PP tool) are also reported in Table 2.2. Observed electron mobility levels (ranging 76 to 126 cm^2/Vs) are lower than those reported in literature for similar electron concentrations (200 to 300 cm^2/Vs, [29]). At least to some extent, this is attributed to excess inactive As, acting as scattering sites.

2.3.2 Conclusions

In the previous section, arsenic was studied as possible n-type dopant in Ge. Ultra shallow arsenic junctions in Ge were fabricated using millisecond laser anneal (LSA) with peak wafer temperatures up to 900 °C. Significant in-diffusion was observed for samples annealed at 800 and 900 °C, yielding a box-like As profile suggesting a mechanism of concentration enhanced diffusion through the formation of arsenic-vacancy (As-V) complexes. A reduced formation of these complexes during LSA in α-Ge samples results in less diffusion and increased electrical activation. An electrical activation of 5.0×10^{19} cm^{-3} was achieved with the 900 °C laser anneal for $X_J = 31$ nm and $R_{sh} = 308$ Ω/sq. with $\mu_H = 126$ cm^2/Vs. Finally, LSA annealing is observed to result in full recrystallization of the amorphized Ge layer.

2.4 Benchmarking

In this section, junctions fabricated in this chapter are benchmarked with respect to results available in literature and the High Performance ITRS requirements for VLSI technology nodes [74, 75]. Additionally, the electrical activation requirements for ultra shallow junctions (USJ) in silicon and germanium will be discussed.

2.4.1 Electrical Activation Requirements

The maximum active concentration level is often used as a measure to compare different fabrication techniques for shallow junctions, since, unlike the sheet resistance R_{sh}, this quantity does not depend on the junction depth X_J itself. Although

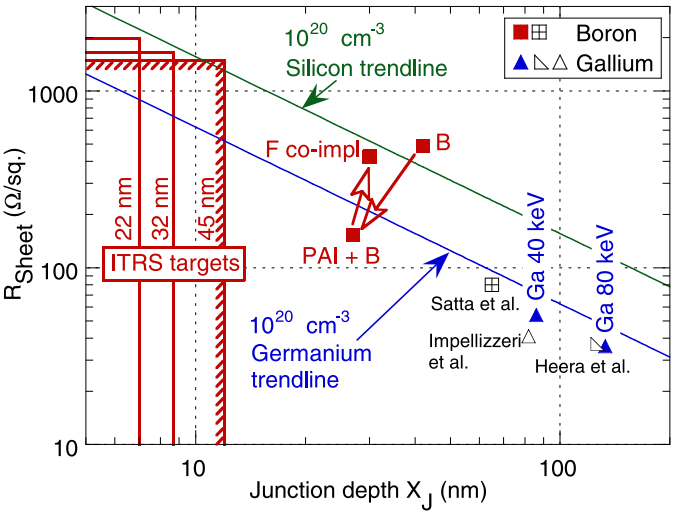

Fig. 2.11 p-Type junction sheet resistance as a function of junction depth for various junctions in Germanium. Trend lines for ideal box-like profiles are added for Si and Ge, along with ITRS targets for the 45, 32 and 22 nm nodes

useful, it remains a poor metric when comparing junctions in different materials. The reason for this is that R_{sh} at a given X_J (i.e. in a given technology) depends not only on the number of charge carriers, but also on the mobility. For an ideal box-like junction, the sheet resistance is given by:

$$R_{sh} = \frac{1}{q\mu(N_{ACT})N_{ACT}X_J} \tag{2.1}$$

Using Eq. (2.1), one can calculate that a p-type junction in Si with $N_{ACT} = 4 \times 10^{20}$ cm^{-3} ($\mu_{\mathrm{Si,h}}(N_{ACT} = 4 \times 10^{20}) = 24$ cm^2/Vs, [34]) has about the same sheet resistance as a Ge junction with a four times lower $N_{ACT} = 1 \times 10^{20}$ cm^{-3} because of the higher hole μ in this material ($\mu_{\mathrm{Ge,h}}(N_{ACT} = 1 \times 10^{20}) = 100$ cm^2/Vs, [50]). In turn, an n-type junction in $In_{0.53}Ga_{0.47}As$ with an active concentration of only $N_{ACT} = 4 \times 10^{18}$ cm^{-3} has the same R_{sh} as an n-type Si junction, with 4×10^{20} cm^{-3} ($\mu_{\mathrm{Si,e}}(N_{ACT} = 4 \times 10^{20}) = 30$ cm^2/Vs, [86]) because of the high electron mobility in this material ($\mu_{\mathrm{In_{0.53}Ga_{0.47}As,e}}(N_{ACT} = 4 \times 10^{18}) = 3000$ cm^2/Vs, [110]). These considerations, among others, make the quantity N_{ACT}, while useful for other purposes, less suited for a benchmarking exercise focussed on the integration of USJ in VLSI logic when comparing different semiconductors.

2.4.2 Benchmarking of USJ in Germanium

The benchmarking of junctions in Ge will be performed using R_{sh} and X_J. R_{sh} is measured directly using a sheet resistance probing technique such as 4PP, VPS or

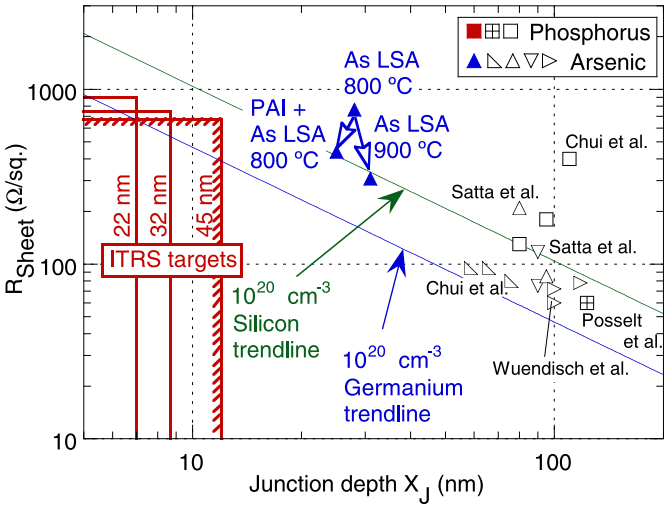

Fig. 2.12 n-Type junction sheet resistance as a function of junction depth for various junctions in Germanium. Trend lines for ideal box-like profiles are added for Si and Ge, along with ITRS targets for the 45, 32 and 22 nm nodes

μ4PP). X_J is taken as either X_J from SIMS-measurements at a concentration level of 4×10^{18} cm^{-3} or the reported metallurgical X_J (whichever one is smaller). This limits the comparison with literature to those references that actually report R_{sh} and X_J or allow their direct extraction (e.g. from the figures). Some authors have used the Spreading Resistance Probing technique (SRP) to characterize dopant activation. Still, calculating R_{sh} from an SRP profile can result in rather large error bars on the result. Consequently, those R_{sh} values will not be included.

2.4.2.1 p-Type Junctions

For p-type junctions, this results in the R_{sh}–X_J plot in Fig. 2.11. The graph includes literature references for B-junctions [125] and for Ga-junctions [51, 70] in Ge, as well as our own results which were discussed in Sects. 2.2.2 (Boron) and 2.2.1 (Gallium). In addition to these data points, the calculated sheet resistance values were included for an ideal box-like p-type junction in Si and Ge ($N_{ACT} = 1 \times 10^{20}$ cm^{-3}) with varying X_J. Finally, the ITRS targets for the 45, 32 and 22 nm technology nodes [74, 75] were added. While the majority of the reported Ge junctions are still a lot deeper than the targets, their electrical activation is equivalent to ideal junctions with N_{ACT} well above 10^{20} cm^{-3}. This graph also underlines the importance of the results obtained in Sect. 2.2.2, where a 27 nm junction was fabricated with a high concentration of electrically active B using SPER and RTA-anneal. If this trend can be maintained and similar active concentration levels can be achieved in even shallower junctions, the sheet resistance of these p-type junctions would be 3–4 times lower than the corresponding ITRS targets.

2.4.2.2 n-Type Junctions

For n-type junctions, a similar R_{sh}–X_J plot was made (Fig. 2.12). This graph includes literature references for p-junctions [24, 117] and for As-junctions [24, 124, 125, 156] in Ge, as well as our own results for As junctions (which were discussed in Sect. 2.3.1). Calculated sheet resistance values were included for an ideal n-type box-like junction in Si and Ge ($N_{ACT} = 10^{20}$ cm^{-3}) with varying X_J. Finally, the ITRS targets for the 45, 32 and 22 nm technology nodes [74, 75] were added. Note that the required R_{sh} values are lower, since the electron mobility exceeds the hole mobility, giving rise to a lower R_{sh} for a given N_{ACT} (see Eq. (2.1)). The n-type junctions found in literature are all deeper than 60 nm. Their sheet resistance is higher than that of an ideal n-type box-like profile ($N_{ACT} = 10^{20}$ cm^{-3}). Using LSA annealing, As junctions were successfully scaled to the $X_J = 20$–30 nm range (Sect. 2.3.1). Nevertheless, it is clear that scaling X_J while maintaining (or preferably improving) the electrical activation is required to fulfill ITRS targets. Unlike p-type dopants in Ge, the higher diffusivity and lower electrical activation of P and As complicates n-type USJ fabrication in Ge.

2.4.3 Conclusions

In the previous section, the electrical activation requirements for ultra shallow junctions (USJ) were discussed. It was found that the electrically active doping concentration requirements in materials which possess a higher carrier mobility than silicon can be much lower (keeping R_{sh} and X_J constant). Taking ideal Si junctions with an active carrier concentration of 4×10^{20} cm^{-3} as a reference, similar R_{sh} values can be obtained in Ge with a $4\times$ lower N_{ACT}, and in $In_{0.53}Ga_{0.47}As$ with a $100\times$ lower N_{ACT}. As such, high mobility materials offer opportunities to reduce parasitic series resistance in MOSFETs, increasing drive current for scaled devices.

Using R_{sh}–X_J plots, the Ge junctions fabricated in this chapter were benchmarked against recent literature results and the ITRS targets for the upcoming technology nodes:

- *For p-type junctions*, a rather high electrically active dopant concentration level was seen for B and Ga junctions (up to 6×10^{20} cm^{-3}, [70]). This level is maintained in shallow junctions (down to $X_J = 27$ nm, 4×10^{20} cm^{-3}). If this trend can be upheld, the sheet resistance of p-type junctions in Ge would be 3–4 times lower than the ITRS targets for the corresponding technology nodes.
- *For n-type junctions*, a lower electrically active dopant concentration level is observed for P and As junctions than for the p-type junctions (10^{19} cm^{-3}-range, [24]), despite the use of more advanced annealing techniques such as FLA and LSA. While an active concentration level of 5×10^{19} cm^{-3} has now been achieved in shallow junctions ($X_J = 25$–31 nm), further improvements are required to meet the n-type ITRS targets.

2.5 Summary and Conclusions

The goal of this chapter was to investigate the fabrication of (shallow) junctions in Ge. To this end, gallium and boron were considered as possible p-type dopants while arsenic was used to fabricate n-type junctions:

Gallium was implanted in crystalline and preamorphized Ge. After a 60 s, 550 °C RTA, a high electrically active dopant concentration level of 4.4×10^{20} cm^{-3} was observed. This study also revealed an increased Ga diffusivity in the amorphous Ge phase. Cross-sectional TEM analysis showed that the recrystallization (SPER) of the amorphous Ge layer is about 3× slower in samples which received a deep pre-amorphization implant (PAI).

Boron junctions were also fabricated showing similar high electrically active dopant concentration levels (4×10^{20} cm^{-3}). The lower implant energy used in this study allowed reducing the junction depth down to 27 nm. In order to achieve an efficient incorporation of Boron into the Ge lattice, a PAI is required, combined with SPER during the RTA anneal. Co-implanting B junctions with F was shown to degrade junction properties: increased B diffusion and resulting dose loss during the RTA anneal yields a 2× lower electrically active concentration level.

Arsenic was studied as an n-type dopant in Ge. Millisecond laser annealing (LSA) was used to activate the implanted arsenic in an attempt to reduce the concentration-enhanced diffusion and resulting dopant deactivation, commonly observed with n-type dopants in Ge. Significant diffusion was however still present in samples annealed at 800 and 900 °C. Furthermore, the box-like profile of the resulting As junctions suggests that the observed diffusion and deactivation during LSA still occurs through the same mechanism of mobile Arsenic-Vacancy complexes. Despite these issues, an electrically active concentration level of 5.0×10^{19} cm^{-3} was achieved with a 900 °C LSA for $X_J = 31$ nm and $\mu_H = 126$ cm^2/Vs following As I/I into c-Ge wafers. Cross-sectional TEM analysis showed full, defect-free recrystallization of the amorphized Ge layer during LSA provided the wafer reaches a peak temperature of 700 °C.

In order to compare the results obtained to the existing Si literature results, electrical activation requirements for ultra shallow junctions (USJ) were discussed. Calculations showed that the required electrically active doping concentration in high-mobility materials can be significantly lower than that in silicon. Taking an ideal Si junction with an active carrier concentration of 4×10^{20} cm^{-3} as a reference, similar R_{sh} values can be obtained in Ge with a 4× lower N_{ACT}, and in $In_{0.53}Ga_{0.47}As$ with a 100× lower N_{ACT}. As such, high mobility materials offer opportunities to reduce parasitic series resistance in MOSFETs, increasing drive current for scaled devices.

Finally, the Ge junctions fabricated in this chapter were benchmarked against recent literature results and the high-performance ITRS targets for the upcoming technology nodes. p-Type junctions using B and Ga in Ge were shown to combine high

N_{ACT} with diffusionless behavior under certain conditions. Consequently, while junction depths were still deeper than ITRS targets, it seems highly likely that junction depths can be reduced further by simply reducing the I/I energy. Provided the current N_{ACT} can be maintained, sheet resistance of B and Ga p-type junctions in Ge would be 3–4 times lower than the targets for the upcoming technology nodes (45, 32 and 22 nm). In contrast, a lower N_{ACT} was observed for P and As junctions in Ge, in combination with significant concentration-enhanced diffusion. So far, even more advanced annealing techniques such as FLA and LSA have failed to produce active dopant concentration levels matching those achieved with p-type dopants in combination with a sufficiently low X_J. Even though, using LSA, active concentration levels close to the ITRS requirements were obtained, further improvements are required to meet n-type junction targets in Ge.

Appendix

A.1 Thermal Laser Anneal—sprocess Simulation Parameters

These are the parameters used for the thermal laser annealing simulations in this work. The syntax below corresponds to the 2010.03 release of sprocess [128]. Default Si parameters are repeated as well for reference.

```
SILICON
Potential ni [expr pow([simGetDouble Diffuse tempK],1.5)
      *[Arr 2.16e16 [expr 0.36-5.12e-8*pow([simGetDouble
      Diffuse tempK],2)] ]]
Absorptivity  0.5*(1.9e-20*(Temperature ^ 1.5)
      *(1.0e15 + [pdbDelayDouble Silicon Potential ni])) + 900.0
Emissivity  1.0
SpecificHeatCapacity  1176 + Temperature
      * (1.3e-4*Temperature - 0.252) - 1.19e5 / Temperature
ThermalConductivity  0.01 * (-73.85 + Temperature
      * (-1.36e-5*Temperature + 5.72e-2) + 6.21e4 / Temperature)



GERMANIUM
 ## absorptivity
Potential ni [expr pow([simGetDouble Diffuse tempK],1.5)
      *[Arr 2.16e16 [expr 0.36-5.12e-8*pow([simGetDouble
      Diffuse tempK],2)] ]]
Absorptivity  0.5*(1.9e-20*(Temperature ^ 1.5)
      *(1.0e15 + [pdbDelayDouble Silicon Potential ni])) + 900.0
Emissivity  0.1\
SpecificHeatCapacity  347.6 + Temperature
      * (1.45e-5*Temperature - 0.00995) - 13921 / Temperature
ThermalConductivity  0.0169 * (-38.715 + Temperature
      * (-2.94e-5*Temperature + 5.90e-2) + 1.76e4 / Temperature)
```

http://www.springer.com/978-94-007-6339-5

High Mobility and Quantum Well Transistors
Design and TCAD Simulation
Hellings, G.; De Meyer, K.
2013, XVIII, 140 p., Hardcover
ISBN: 978-94-007-6339-5